Supplementary information

Surface protolytic properties characterization of hydroxyapatite and titanium dioxide nanoparticles.

Ekaterina Kukleva[1], Petra Suchánková[1], Karel Štamberg[1], Martin Vlk[1], Miroslav Šlouf[2], Ján Kozempel[1*]

[1] *Czech Technical University in Prague, Faculty of Nuclear Sciences and Physical Engineering, Department of Nuclear Chemistry, Břehová 7, 11519 Prague 1, Czech Republic*

[2] *Institute of Macromolecular Chemistry, Czech Academy of Sciences, Heyrovský square 2, 16206 Prague 6, Czech Republic*

*E.mail: jan.kozempel@fjfi.cvut.cz

Theoretical basis for titration modelling and evaluation

Protonation and sorption processes taking part on the edge sites can be described (modeled) by several types of Surface Complexation Models (*SCM*)[1,2] from which the following models are the most utilized: Constant Capacitance Model (*CCM*), Diffusion Double Layer Model (*DLM*), and non-electrostatical Chemical Equilibrium Model (*CEM*). The processes taking part on layer sites are always described by classical Ion Exchange Model (*IExM*). Since hydroxyapatite can substitute Ca^{2+} for other cations, the necessity to involve *IExM* into HAp modelling seems to be obvious.

Modeling by *IExM* could be, but does not have to be taken into account in order to find out the most accurate fit. Therefore, six model combinations should be tested, namely, *CCM, CCM+IExM*, *DLM, DLM+IExM, CEM* and *CEM+IExM*. General parameters characterizing the nHAp and $nTiO_2$ can be found in RES[3]T- Database[3], which is constantly updated. Especially, with regards to $nTiO_2$, there are different values of surface protolysis and sites density data taken from more than 20 articles. These values differ in the way of $nTiO_2$ preparation and in its specific surface area. In the case of nHAp, in contrast to $nTiO_2$, only 4 articles are cited. However, according to the literature[3] the edge site density is approx. 0.3 mol·kg^{-1} for $nTiO_2$, and approx. 3 mol·kg^{-1} for nHAp, which points to its potentially very good sorption.

The reactions taking place on the surface of nHAp or $nTiO_2$ can be described by three equations (1) - (3). The first two are protonation reactions being in progress on edge sites, the third one describes the ion-exchange on layer sites.

$$\equiv SO^- + H^+ \Leftrightarrow \equiv SOH \quad (1)$$

$$\equiv SOH + H^+ \Leftrightarrow \equiv SOH_2^+ \quad (2)$$

$$\equiv XNa + H^+ \Leftrightarrow \equiv XH + Na^+ \quad (3)$$

The equilibrium constants for reactions (1) - (3), K_1, K_2 and K_{ex} respectively are given by equations (4) - (6):

$$K_1 = \frac{[SOH]}{[SO^-][H^+]} \quad (4)$$

$$K_2 = \frac{[SOH_2^+]}{[SOH][H^+]} \quad (5)$$

$$K_{ex} = \frac{[XH][Na^+]}{[XNa][H^+]} \quad (6)$$

The balance equations of charge densities on edge sites ($\sum SOH$) (7) and layer sites ($\sum X$) (8) have to be taken into account in order to provide correct description of surface reactions:

$$\sum SOH = [SOH] + [SO^-] + [SOH_2^+] \quad [\text{mol.kg}^{-1}] \quad (7)$$

$$\sum X = [XH] + [X^-] = [XH] + [XNa] \quad [\text{mol.kg}^{-1}] \quad (8)$$

It is important to notice that the edge sites of the nHAp are characterized as ≡*POH* functional groups[4], while $nTiO_2$ edge sites are formed by ≡*SOH* groups.

The modeling procedure of the titration system can be characterized as follows: the total surface charge density, $(Q_{cal})_i$, in the *i*-th point of the titration curve equals the sum of charge density on the edge sites, $(Q_{ES})_i$, and on the layer sites, $(Q_{LS})_i$.[1,5] Therefore, it holds:

$$(Q_{cal})_i = (Q_{ES})_i + (Q_{LS})_i \quad (9)$$

Based on the character of titration curve and equations (10) and (11), the charge density is the function of pH. The values of $(Q_{ES})_i$ and $(Q_{LS})_i$ can be calculated by means of equations (10) and (11), respectively:

$$(Q_{ES})_i = \frac{\sum SOH \cdot \left(K_1 \cdot K_2 \cdot [H^+]^2 + 1\right)}{K_1 \cdot K_2 \cdot [H^+]^2 + K_1 \cdot [H^+]^2 + 1} \quad [\text{mol.kg}^{-1}] \quad (10)$$

$$(Q_{LS})_i = \frac{\sum X \cdot [Na^+]}{[Na^+] + K_{ex} \cdot [H^+]} \quad [\text{mol.kg}^{-1}] \quad (11)$$

The experimental value of the surface charge for *i*-th point of titration curve, $(Q_{ex})_i$, can be obtained using equation (12):

$$(Q_{exp})_i = \frac{V_i \times \left(C_{a,i} - C_{b,i} + [OH^-]_i - [H^+]_i\right)}{m_i} \quad [\text{mol.kg}^{-1}] \quad (12)$$

Where V_i [L] is the total volume of liquid phase; m_i [kg] is the mass of solid phase; $C_{a,i}$ [mol·L^{-1}] and $C_{b,i}$ [mol·L^{-1}] are bulk concentrations of acid (e.g. HNO_3) and sodium hydroxide in liquid phase, respectively, which are given by stock concentrations of acid and base solutions and by their consumptions during titration.

If the values of parameters K_1, K_2, K_{ex}, $\sum SOH$ and

$\sum X$, were sought, some non-linear multi-dimensional regression procedure should be used that deals with the fitting of experimental data, $(Q_{exp})_i$, with model data, $(Q_{cal})_i$. The software product FAMULUS[6] and the proper code P46DNRLG.fm (code package STAMB 2015) based on the Newton-Raphson multidimensional nonlinear regression procedure were used. *WSOS/DF* (weighted

sum of squares of differences divided by number of degrees of freedom) was used as the criterion of goodness-of-fit.[7]

It is necessary to add that the basic assumption of the surface complexation models is the validity of Boltzman equation (13)[1] quantifying the relation between the concentration of *i*-th-component in aqueous phase near the surface (in aqueous layer adhering to the surface), $(C_i)_s$, and its bulk concentration, C_i, (13):

$$(C_i)_s = C_i \cdot exp(-z \cdot \psi \cdot F/(R \cdot T)) \qquad (13)$$

where z is the charge of *i*-th component (valency), ψ [V] is the electrostatic potential, F [C.mol^{-1}] is Faraday constant, R [J·K^{-1}·mol^{-1}] is gas constant and T [K] is the absolute temperature. The following dependences then hold between surface charge, σ [C·m^{-2}], and electrostatic potential, ψ, (14, 15, 16):

$$\sigma = G \cdot \psi \qquad \text{(CCM)} \qquad (14)$$

$$\sigma = 0.1174 \cdot I^{1/2} \cdot sinh(z_i \cdot \psi \cdot F/(2RT)) \qquad \text{(DLM)} \qquad (15)$$

$$\psi = 0 \text{ and } (C_i)_s = C_i \qquad \text{(CEM)} \qquad (16)$$

where G [F·m^{-2}] is the so-called Helmholtz capacitance.

Specific surface area, FTIR, XRPD and TEM

FTIR spectra (**Fig. S1**) have showed the characteristic vibration bands of both studied materials and are described in detail in the article.

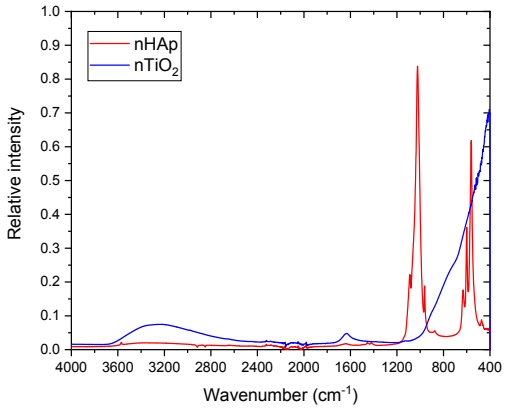

Fig. S1 FTIR spectrum of $nTiO_2$ and nHAp.

Nanohydroxyapatite and $nTiO_2$ diffractograms showed that both samples are single phase and structure of both materials were proven by library data[8] comparison (**Fig. S2**).

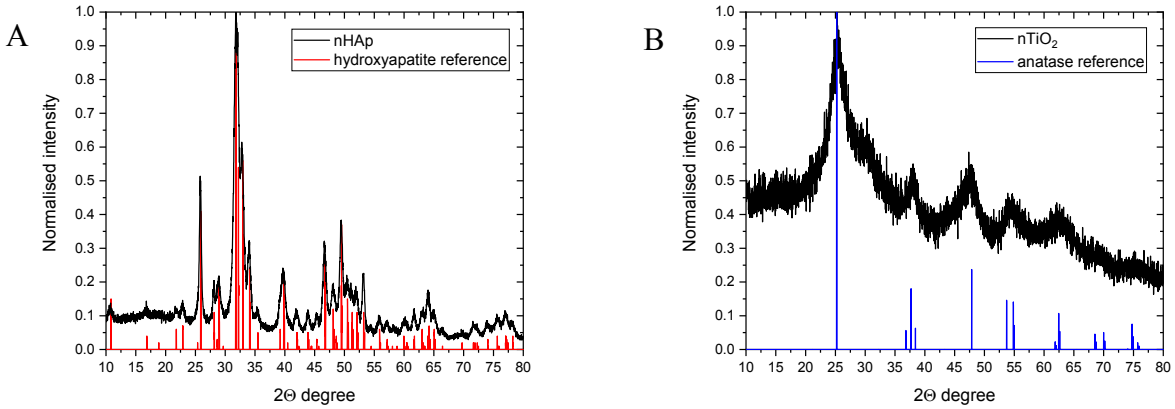

Fig. S2 nHAp (A) and $nTiO_2$ (B) difractograms compared with library records ICDD PDF-2 database[8] (version 2013) (HAp – card# 01-071-5048; TiO_2 – card# 01-084-1285).

TEM characterization of nHAp and $nTiO_2$ is shown in **Figs. S3** and **S4**, respectively, and are described in detail in the article.

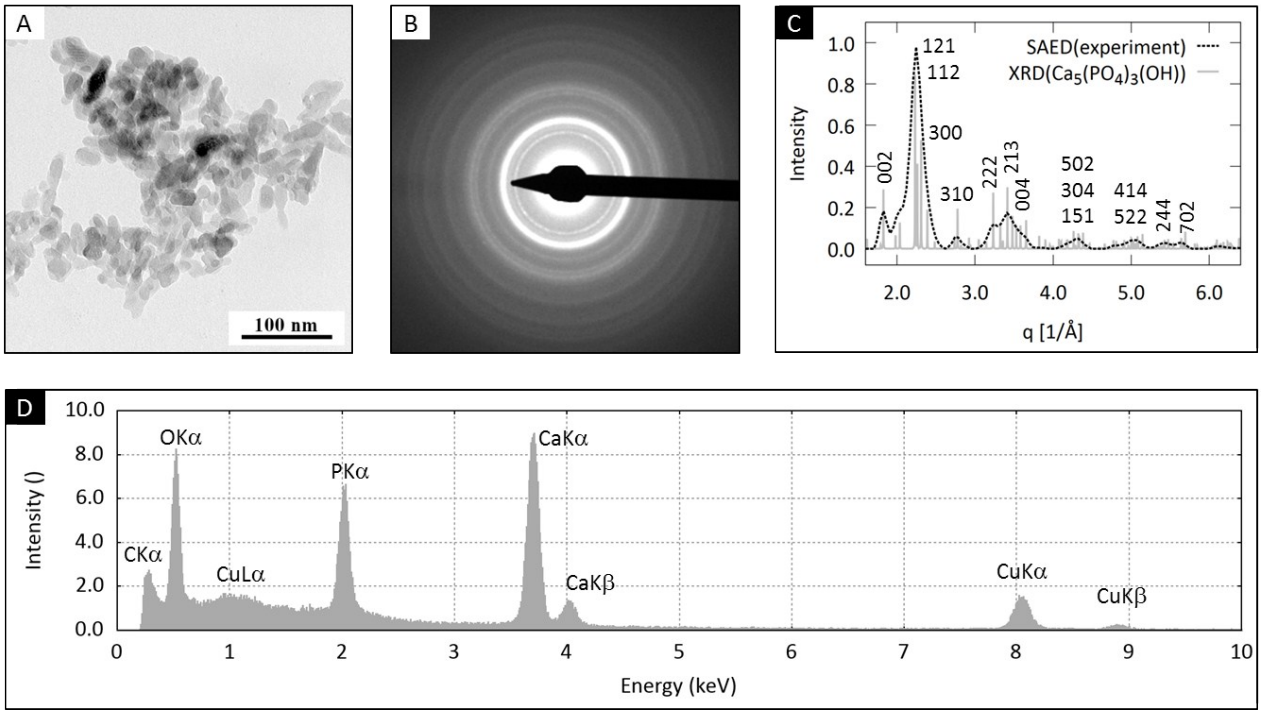

Fig. S3 TEM analysis of nHAp: A) TEM/BF micrograph showing the size and shape of nHAp, B) TEM/SAED diffraction pattern, C) comparison of the experimental SAED pattern and theoretically calculated XRD pattern of hydroxyapatite, D) TEM/EDX spectrum of nHAp.

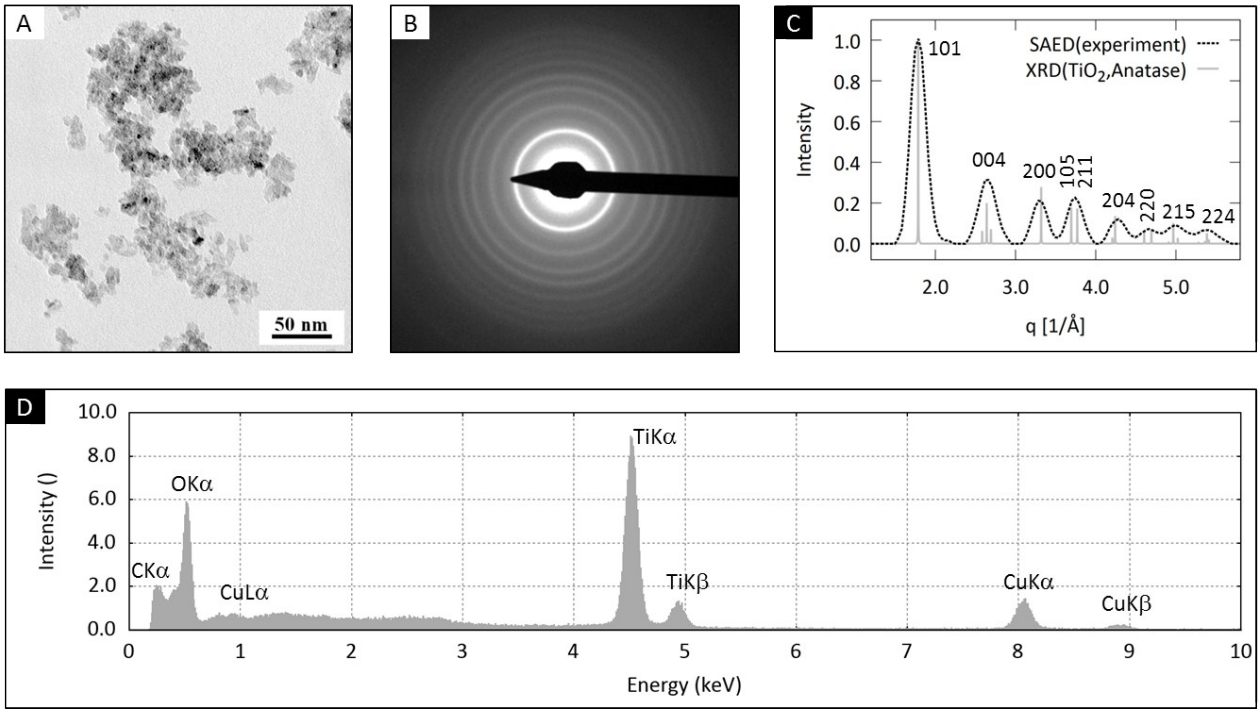

Fig. S4 TEM/SAED analysis of $nTiO_2$: A) TEM/BF micrograph showing the size and shape of $nTiO_2$, B) TEM/SAED diffraction pattern, C) comparison of the experimental SAED pattern and theoretically calculated XRD pattern of anatase, D) TEM/EDX spectrum of $nTiO_2$.

Estimate of crystallite size from electron diffraction patterns

The crystallite size was estimated from Scherrer equation that relates average crystallite size, L, with the full width of the diffraction peaks at half-maxima of the peaks ($FWHM(q)$)[9]:

$$L = (K \cdot 2\pi)/FWHM(q) \quad (17)$$

The constant K is usually set equal to 0.89,[10] while q represents diffraction vector ($q = 4\pi \cdot \sin(\theta)/\lambda$, where θ is the diffraction angle and λ is the wavelength of diffracting electrons).[9,10]

Image analysis: calculation of particle size distribution and specific surface area

Image analysis of TEM/BF micrographs consisted in interactive measurement of particles using ImageJ[11] and further processing of the measured values using our program MDISTR[12,13]. For each sample, more than 100 particles were measured with ImageJ. For each particle, we measured both minimal and maximal projected lengths (i.e. the smallest and the biggest diameter of the particle; morphological descriptors: *MaxFeret* and *MinFeret*). From the projected lengths we estimated average particle size (morphological descriptor: *EqDiameter*; (18)) and average asphericity (morphological descriptor: *Elongation*; (19)):

$$EqDiameter \approx 1/2 \cdot (MaxFeret + MinFeret) \quad (18)$$

$$Elongation = MaxFeret/MinFeret \quad (19)$$

In the next step, we employed our own MDISTR software package to calculate histograms, plot particle size distributions and total number and total surface area of the particles with given

distribution and total mass. If the MDISTR program is instructed to calculate total surface area of the investigated particles with total mass = 1 g, we obtain specific surface area that should be equal to the experimentally determined specific surface area from BET experiments (which is usually expressed in m^2/g). The MDISTR package was originally developed for analysis of synthetic polymer systems with complex morphologies[12-14], but later it has been extended to calculate also specific surface areas, considering various corrections due to particle shapes and/or particle surface roughness. Comparison of specific surface area models and BET experiments is summarized in **Fig. S5**.

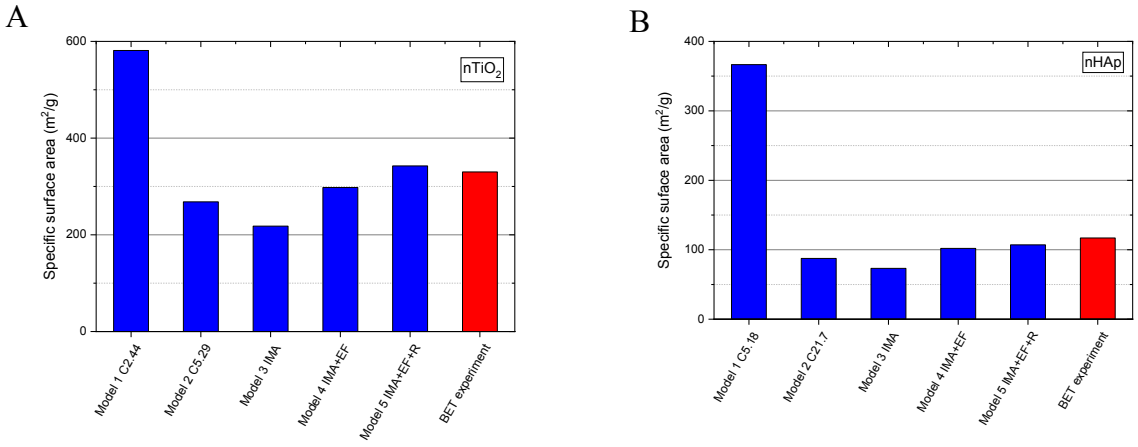

Fig. S5 Comparison of specific surface area models and BET experiment, A) nTiO2; B) nHAp; the model-based values (blue columns) were calculated with MDISTR software[12 -14].

The HAp and TiO_2 morphological descriptors, particle size distributions and overall semi-quantitative characteristics of the observed nanoparticles (such as their roughness estimated from their shapes in higher magnification TEM/BF micrographs), were employed in the calculation of the specific surface area of the nanoparticles. The final calculated values from MDISTR program (Tab. 2 in the article) were compared with the experimentally determined specific surface areas from BET experiments (**Fig. S5**). The agreement between theoretical calculations based on TEM data including all corrections and the experimental results from BET experiments was very good. In both samples, the SAED-based crystallite sizes resulted in overestimation of specific surface area in comparison with BET experiments (**Fig. S5**, compare results of Model 1 and BET experiments), which implied that SAED-based crystallite sizes were too small, resulting in too high numbers of particles with too high specific surface area. This could be attributed to two facts: Firstly, the Scherrer equation is just an approximate relation, which yields lower bound of the volume-averaged crystallite size. Secondly, certain fraction of the nanocrystals (observed in TEM/BF micrographs) could be composed of two or more crystallites (whose size is estimated from TEM/SAED diffractograms). The above argument is confirmed by the fact that he estimate of specific surface area based on average crystal sizes which come from image analysis of TEM/BF micrographs was significantly closer to reality (**Fig. S5**, compare results of Model 2 and BET experiments). However, calculation with spherical particles with uniform size (constant particle size distribution) is just an approximation resulting in slight underestimation of specific surface area. We have to take into account the real particle size distribution (**Fig. S5**, Models 3), correction for particle elongation and flattening (**Fig. S5**, Models 4), and finally also correction for particle surface roughness (**Fig. S5**, Models 5). The corrections that are inserted as user-defined input, are either directly calculated

(elongation) or merely estimated (flattening, roughness) from the shapes and/or contrast of nanoparticles in the TEM/BF micrographs.[12] The change from uniform, constant distribution (**Fig. S5**, Models 2) to real, broadened distribution (**Fig. S5**, Models 3) is always accompanied by a decrease in total number of particles (and, as a result, also by a decrease of total surface area) because in the real, broadened distribution the bigger particles occupy more volume and less surface than smaller particles.[12,14] The introduction of elongation and flatness corrections (**Fig. S5**, Models 4) does not change the total number of particles, but somewhat increases their total surface area because the elongated and/or flat particles exhibit larger surface area than equivalent spherical particles. The introduction of roughness correction (**Fig. S5**, Model 5) further increases the total surface area, as the rough particles logically exhibit larger surface than smooth spheres, ellipsoids, or platelets. Although all corrections introduced into the program are rather approximate or even semi-quantitative, the final values were in a very good agreement with the specific surface areas from BET experiments, which confirms both the correctness of our MDISTR program package and reliability of our TEM analyses.

Supplementary References

1 H. Filipská and K. Štamberg, *Acta Polytech.*, 2005, 45(5), **11-18**

2 J. Lützenkirchen, *Surface complexation modelling*, Academic Press, Elsevier Ltd., London, 2006

3 RES3T / Rossendorf Expert System for Surface and Sorption Thermodynamics, https://www.hzdr.de/db/res3t.login, (accessed January 2018)

4 B. Sandrine, N. Ange, B.A. Didier, C. Eric and S. Patrick, *J. Hazard. Mater.*, 2007, **139(3)**, 443-446

5 H. Wanner, Y. Albinson, O. Karnland, E. Wieland, P. Wersin and L. Charlet, *Radiochim. Acta*, 1994, **66/67**, 157-162

6 L. Dvořák, T. Ledvinka and M. Sobotka, FAMULUS 3.1, Computer equipment, Prague, 1991

7 A.L. Herbelin and J.C. Westall, FITEQL – a computer program for determinationof chemical equilibrium constants from experimental data. Version 3., Report 96-01. Department of Chemistry, Oregon State University, Corvalis, Oregon, USA, 1996

8 ICDD PDF-2 Database - version 2013, ISDD, USA

9 B. Ingham and M.F. Toney, in *Metallic Films for Electronic, Optical and Magnetic Application*, ed. K. Barmak and K. Coffey, Elsevier, New York, 2014, chapter 1: X-ray diffraction for characterizing metallic films, 3-38

10 B. Fultz and J. Howe, *Transmission electron microscopy and diffractometry of materials*, Springer, Berlin, 2008

11 C.A. Schneider, W.S. Rasband and K.W. Eliceiri, *Nat Methods*, 2012, **9(7)**, 671–675

12 J. Gallo, M. Slouf and S.B. Goodman, *J. Biomed. Mater. Res., Part B*, 2010, **94B(1)**, 171-177

13 M. Slouf, A. Ostafinska, M. Nevoralova and I. Fortelny, *Polym. Test.*, 2015, **42**, 8–16

14 P. Fulín, D. Pokorný, M. Slouf, M. Lapčíková, E. Pavlova and E. Zolotarevová, *Acta Chir. Orthop. Traumatol. Cech.*, 2011, **78(2)**, 131-7